

Empirical stability criteria for 3D hierarchical triple systems I: Circumbinary planets

NIKOLAOS GEORGAKARAKOS,^{1,2} SIEGFRIED EGGL,³ MOHAMAD ALI-DIB,² AND IAN DOBBS-DIXON^{1,2}

¹*Division of Science, New York University Abu Dhabi, PO Box 129188, Abu Dhabi, UAE*

²*Center for Astrophysics and Space Science (CASS), New York University, Abu Dhabi, PO Box 129188, Abu Dhabi, UAE*

³*Department of Aerospace Engineering / Department of Astronomy / NCSA CAPS, University of Illinois at Urbana-Champaign
Urbana, IL, USA*

ABSTRACT

In this work we revisit the problem of the dynamical stability of hierarchical triple systems with applications to circumbinary planetary orbits. We carry out more than $3 \cdot 10^8$ numerical simulations of planets between the size of Mercury and the lower fusion boundary (13 Jupiter masses) which revolve around the center of mass of a stellar binary over long timescales. For the first time, three dimensional and eccentric planetary orbits are considered. We explore systems with a variety of binary and planetary mass ratios, binary and planetary eccentricities from 0 to 0.9 and orbital mutual inclinations ranging from 0° to 180° . The simulation time is set to 10^6 planetary orbital periods. We classify the results of those long term numerical integrations into three categories: stable, unstable and mixed. We provide empirical expressions in the form of multidimensional, parameterized fits for the two borders that separate the three dynamical domains. In addition, we train a machine learning model on our data set in order to have an alternative tool of predicting the stability of circumbinary planets. Both the empirical fits and the machine learning model are tested against randomly generated circumbinary systems with very good results regarding the predictions of orbital stability. The empirical formulae are also applied to the Kepler and TESS circumbinary systems, confirming the stability of the planets in these systems. Finally, we present a REST API with a web based application for convenient access of our simulation data set.

Keywords: Binary stars (154) — Celestial Mechanics(211) — Dynamical evolution (421) — Exoplanet dynamics (490)

1. INTRODUCTION

Binary stars make up a considerable fraction of the stellar population in our galactic neighborhood (e.g. [Raghavan et al. 2010](#); [Janson et al. 2012](#); [Offner et al. 2022](#)). Despite the significant technical challenges of observing exoplanets in such environments, a number of them have already been discovered¹. Some of those exoplanets were found to be in circumbinary orbital configurations, i.e. the planet orbits the center of mass of the stellar binary. A vital part of ruling out false positives in the search for exoplanets is the assessment of whether or not predicted orbital configurations are dynamically stable (e.g. [Kostov et al. 2021](#)). This is especially true for circumbinary planets since they experience significant gravitational perturbations from the stars they orbit. Besides the great practical use, stability studies can also be informative in various problems related to planet formation (e.g. [Childs & Martin 2021](#); [Kenyon & Bromley 2021](#)) or habitability (e.g. [Georgakarakos et al. 2021](#); [Georgakarakos 2022](#)).

The problem of determining stable orbit configurations with three gravitating bodies, is one of the classical problems in Celestial Mechanics. Over centuries, many have attempted to find solutions to this problem (e.g. see [Georgakarakos 2008](#)). While general analytical solutions do exist, they can be impractical ([Sundman 1913](#)). Hence, authors have recently focused on investigating the stability of configurations of particular astronomical and astrophysical interest, such as triple stellar and planetary systems around binary stars with the aim of deriving suitable criteria for determining the dynamical fate of those systems. A variety of methods and tools have been used to achieve this goal, i.e. analytical

¹ NASA Exoplanet Archive(<http://exoplanetarchive.ipac.caltech.edu>).

methods (e.g. [Shevchenko 2015](#)), numerical approaches (e.g. [Doolin & Blundell 2011](#)) and more recently Machine Learning (e.g. [Lam & Kipping 2018](#)). Numerical solutions of ordinary differential equations are the backbone of the latter two approaches. Almost half a century ago, [Harrington \(1977\)](#) carried out a limited number of numerical simulations of three body systems and suggested a simple stability criterion based on his results. Later, [Dvorak \(1986\)](#), based on numerical simulations of circumbinary planets on initially circular and coplanar orbits around an equal mass binary star, suggested parabolic fits that separate dynamically stable and unstable regions in which a planet could or could not survive, respectively. This work was extended to binaries with unequal stellar components a few years later ([Dvorak et al. 1989](#)) and to non-coplanar orbits by [Pilat-Lohinger et al. \(2003\)](#). Finally, the work of [Dvorak \(1986\)](#) was recently extended to retrograde orbits ([Hong & van Putten 2021](#)).

The most widely used empirical criterion has been the one presented in [Holman & Wiegert \(1999\)](#). Therein, the authors investigated the dynamical stability of planets in binary systems, either in S-type (the planet orbits one of the stars) or in P-type (the planet orbits both stars) configuration. They performed numerical simulations of massless particles on initially circular and prograde orbits around the binary or around one of the stars, in the binary plane of motion and with different initial orbital longitudes. A variety of binary masses and eccentricities was considered. Similar work on circumbinary planets was done by [Quarles et al. \(2018\)](#).

In this paper we aim to extend and homogenize the results of previous studies on the dynamical stability of circumbinary planetary orbits. We remedy the limitations and inconsistencies that arise from combining stability estimates from different works by carrying out a self-consistent set of numerical simulations over the longest timescale ever used in such studies. The most notable differences of this work compared to the research cited above are: i) a comprehensive scan of 3D angular momentum directions of the planet. We investigate coplanar and non-coplanar (even perpendicular) configurations with prograde and retrograde orbits; ii) we investigate systems where the planetary body has some mass - it is not approximated as a massless particle, iii) a comprehensive scan of orbital eccentricities, where the planet can be initially on a circular or on an elliptic orbit (with up to 0.9 eccentricity), and iv) a substantially longer timescale of system evolution, since we propagate the system for 10^6 planetary orbital periods, which is at least 100 times longer than [Holman & Wiegert \(1999\)](#) and in certain cases, especially for eccentric planetary orbits, that number is of the order of several thousands.

Similarly to [Dvorak \(1986\)](#), we construct empirical fits of two borders of specific stability behaviour: an upper critical border, above which all starting positions for the planet along its orbit remain stable over the integration time and a lower critical border, below which the planetary orbit is unconditionally unstable. In order to show that our results are applicable to real systems, we apply our stability criteria to currently known circumbinary systems. Moreover, we make our stability catalog available to the community in several convenient ways, including through a web-portal and an online application programming interface (API).

The rest of this article is structured as follows: in section 2 we explain the method and setup of our numerical experiments. In section 3 we present our results along with the empirical stability formulae derived by our simulation outcome data. In section 4 we compare our fits against results from random simulations. In section 5, we use Machine Learning to study the problem of circumbinary stability, while in section 6 we apply our fits to real exoplanetary systems discovered by Kepler and TESS. Section 7 briefly describes the online tools we have developed that make our results widely accessible. Finally, we conclude this article with a discussion and a summary of our results.

2. METHODOLOGY

A hierarchical triple system consists of a binary system and a third body on a wider orbit around the center of mass of that binary. The motion of such a system can be pictured as the motion of two binaries: the binary itself (which is called the inner binary) and the binary which consists of the third body and the centre of mass of the inner binary (which is called the outer binary). The problem under investigation here, i.e. the dynamical stability of circumbinary planetary orbits is a special case of a hierarchical triple configuration. The inner binary consists of the two stars, while a planet orbits their center of mass. [Figure 1](#) is a schematic representation of such a system.

In order to study the problem of dynamical stability of circumbinary planets, we made extensive use of numerical simulations. At the heart of our simulations is the regularized, symplectic integrator with time transformation developed in [Mikkola \(1997\)](#). This code is not only symplectic in nature, which guarantees adequate conservation of system energy and angular momentum, it is also one of the few symplectic algorithms that can handle highly eccentric orbits and strong, localized gravitational interactions without loss of accuracy. The code uses Jacobi coordinates, i.e. it calculates the relative position and velocity vectors of the stars and the planet at every time step. The systems

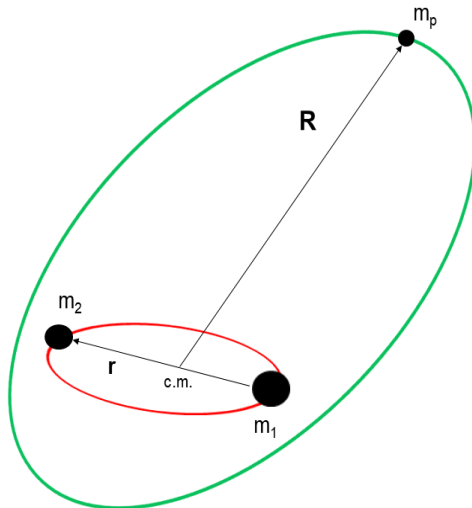


Figure 1. A schematic representation of a circumbinary orbit.

are normalized such that the gravitational constant $G = 1$ and the masses of the binary stars $m_1 + m_2 = 1$. The initial semi-major axis of the binary was also normalized to unity in corresponding units. We convert the output of the integrator to a set of Keplerian orbital elements for the binary stars and the planet.

All systems consist of a stellar binary and a planet on a wider orbit around the binary center of mass. There were no restrictions in the initial orbital configurations, i.e. we investigated circular and eccentric orbits, coplanar and non-coplanar orbits and none of the three bodies was taken to be massless. All the bodies were treated as point masses and Newtonian gravity was the only effect considered.

2.1. Sampled parameter space

Our aim is to be as comprehensive as possible in this study, which entails sweeping all relevant parameters. We make use of two mass parameters,

$$M_b = \frac{m_2}{m_1 + m_2} \text{ and } M_p = \frac{m_p}{m_1 + m_2}, \quad (1)$$

where m_1 and m_2 are the masses of the two stars and m_p is the mass of the planet. The mass parameter space was sampled as follows

$$M_b \in \{0.5, 0.3, 0.1, 0.05, 0.02, 0.01\} \quad (2)$$

and

$$M_p \in \{10^{-2}, 10^{-3}, 10^{-4}, 10^{-5}, 10^{-6}, 10^{-7}\}. \quad (3)$$

As our reference plane, we consider the initial orbital plane of the binary with the x-axis pointing at the direction of the binary longitude of pericenter. Hence, the binary pericenter started at zero in all cases. The choice of the initial mutual inclination between the orbital planes of the binary and that of the planet covers both prograde and retrograde orbits. We sampled values between 0° and 180° with a step of 18° , i.e.

$$I_m \in \{0^\circ, 18^\circ, 36^\circ, 54^\circ, 72^\circ, 90^\circ, 108^\circ, 126^\circ, 144^\circ, 162^\circ, 180^\circ\}. \quad (4)$$

For non-coplanar orbits, the longitude of the ascending node of the planet $\Omega_p \in \{0^\circ, 90^\circ \text{ and } 180^\circ\}$. The planetary longitude of pericenter ϖ_p (when dealing with coplanar orbits) and argument of pericenter ω_p (when working with three dimensional orbits) were given the same values as Ω_p . We considered initially circular and eccentric orbits for both the binary and the planetary orbit. Thus, the eccentricities were sampled as

$$e_b, e_p \in \{0, 0.1, 0.2, 0.3, 0.4, 0.5, 0.6, 0.7, 0.8, 0.9\}, \quad (5)$$

where e_b and e_p are the binary and planetary eccentricity respectively. Initially, the planet was placed at eight different positions with

$$f_p \in \{0^\circ, 45^\circ, 90^\circ, 135^\circ, 180^\circ, 225^\circ, 270^\circ, 315^\circ\}, \quad (6)$$

where f_p denotes the true anomaly of the planet. When the planet was on an initially circular orbit, it was started at the same angular positions around the stellar binary. For eccentric binaries, we used $f_b = 0^\circ$ and $f_b = 180^\circ$, f_b being the true anomaly of the stellar binary. Finally, the integration time was set to 10^6 orbital periods of the planet.

2.2. Working definition of dynamical stability

In the context of this work, a system was classified as dynamically stable when the numerical simulations showed no sign of instability for any initial position of the planet on its orbit over the full time interval, i.e. 10^6 orbital periods of the planet. A system was considered to be unstable if at least one of the following conditions was satisfied: a) either the binary or the planetary orbital eccentricity exceeds unity, b) orbit crossing occurs, c) $a_b/a_{b_0} \leq 0.001$ or $a_b/a_{b_0} \geq 100$, d) $a_p/a_{b_0} \geq 1000$, where a_b and a_p are the binary and planetary semi-major axes respectively and a_{b_0} is the initial binary semi-major axis.

For each set of parameters ($M_b, M_p, I_m, e_b, e_p, \Omega_p, \omega_p, \varpi_p$) we recorded three different stability regimes-areas i) stable motion for all initial true anomaly/angular position combinations, ii) mixed stable-unstable motion with at least one true anomaly/angular position combination being stable and at least one being unstable and iii) unstable motion for all initial true anomaly/angular position combinations. For a given set of parameters, the semi-major axis of the planet where the transition between two of the above mentioned areas of stability-instability behavior takes place is called the critical semi-major axis a^{cr} . Hence, we define two such critical semi-major axes: the outer (or upper) critical semi-major axis, which is the border between regimes (i) and (ii) and the inner (or lower) critical semi-major axis, which is the border between regimes (ii) and (iii). This stability classification scheme was introduced in [Dvorak \(1986\)](#), and is motivated by the fact that nonlinear dynamical systems display extreme sensitivity to changes in initial conditions in regimes that are in - or close to chaotic - domains.

3. RESULTS

A Graphical representation of our results can be found in [Figures 2 and 3](#) which contain plots of the outer critical semi-major axis against the inner one, averaged over the various parameters. The parameter that had the greatest effect on the stability of the systems was the planetary eccentricity (top right panel of [figure 2](#)). High planetary eccentricity values ($e_p > 0.7$) drive the two critical borders far away from the stellar binary. That effect was stronger when combined with moderate to high values of the binary eccentricity. This is to be expected since one of the main drivers of dynamical instability in the hierarchical three body problem is resonance overlap ([Chirikov 1979](#)). The resonance width in such configurations is proportional to both eccentricities and has a strong dependence on the outer eccentricity when the latter becomes large (e.g. [Mardling 2008, 2013](#)).

The binary mass ratio and the mutual inclination seem to have a moderate effect on the location of the two stability borders. As seen in the bottom left panel of [figure 2](#), the smallest value for the binary mass ratio, $M_b = 0.01$ appears to lead to larger areas of stable circumbinary motion. As we progress to higher values of the binary mass ratio, the stable area starts to shrink and it reaches its minimum when the inner binary consists of comparable mass bodies. A hint for this kind of behavior is given by secular evolution. We know for instance that the maximum eccentricity for a circumbinary orbit is proportional to $m_1 m_2 (m_1 - m_2) / (m_1 + m_2)^3$ ([Georgakarakos & Eggl 2015](#)) or, if we express that in terms of the binary mass ratio, to $(2M_b^2 - 3M_b + 1)M_b$. For that kind of binary mass dependence, smaller values of M_b yield smaller values of maximum e_p and probably more stable systems.

When considering the effect of the mutual inclination on circumbinary stability, our simulation outcome confirmed that, generally, retrograde orbits near inclinations of 180° appear to be more stable, i.e. the stability borders were closer to the stellar binary compared to a prograde system with the same parameters (e.g. [Georgakarakos 2008, 2013](#), and bottom right panel of [figure 2](#)). However, and this was seen in previous studies as well (e.g. [Doolin & Blundell 2011](#); [Chen et al. 2020](#)), there were cases where the behavior of the stability border as a function of the mutual inclination did not follow that trend but it was more complicated. [Figure 4](#) provides such an example.

While all bodies in our simulations were massive, we focused on relatively low mass external perturbers that do not exceed one percent of the mass of the inner binary. Consequently, the mass of the outer companion did not have a significant effect on the stability borders (top row of [figure 3](#)). Unsurprisingly, the highest value of $M_p = 0.01$ showed the larger impact, especially for systems where the binary members had a significant mass difference.

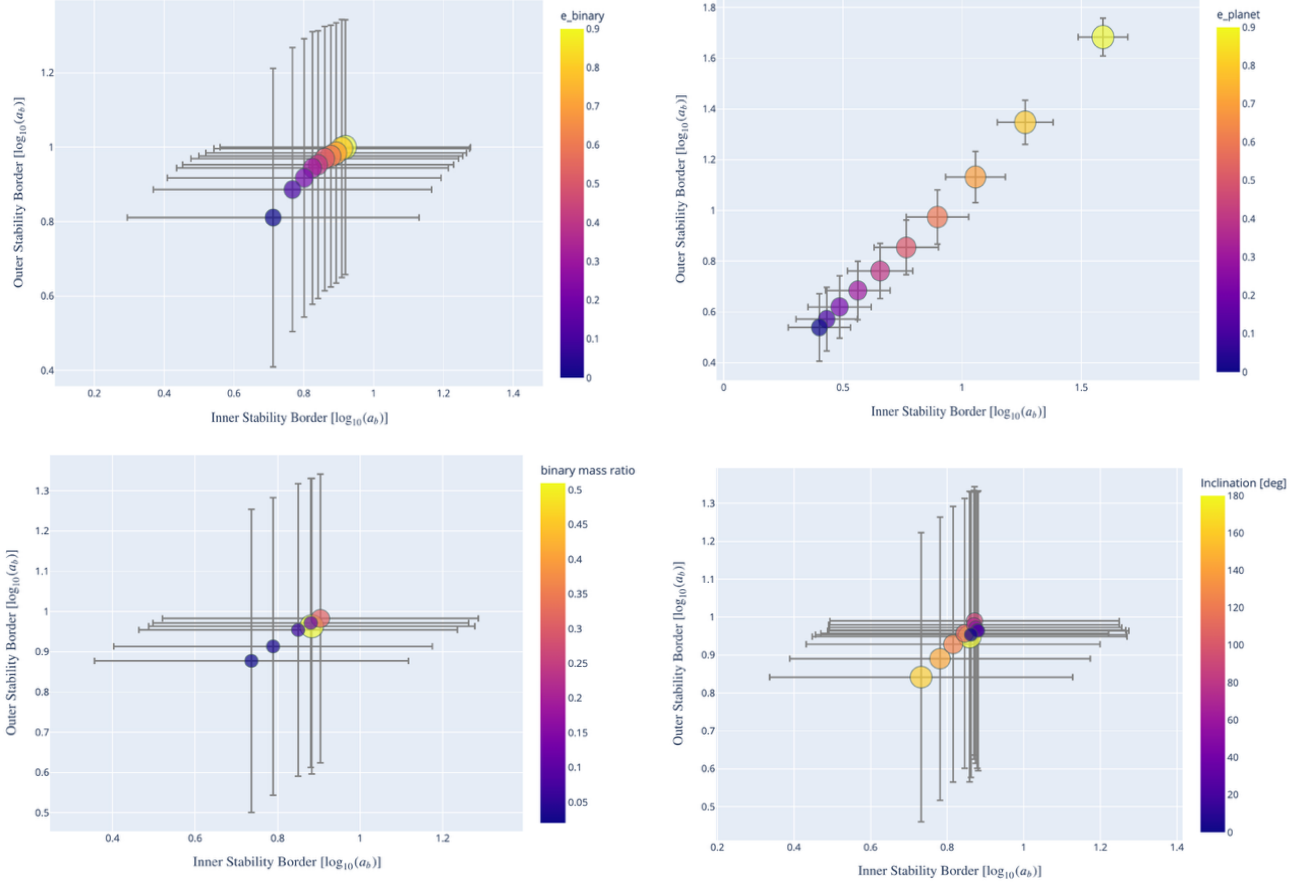


Figure 2. Mean and standard deviation of outer vs inner stability borders in units of \log_{10} of the binary semi-major axis. The color scale refers to the binary orbit eccentricity (top left), the planet’s orbital eccentricity (top right), the binary mass ratio (bottom left), and the mutual inclination (bottom right). Stability limits depend strongly on the planetary orbital eccentricity which accounts for most of the variance in the system. Stability borders also show roughly the same sensitivity to the binary star orbital eccentricity, the binary mass ratio as well as the inclination of the system.

Finally, the slowly evolving angles, i.e. the longitude of the ascending node and the argument of pericenter of the planetary orbit did not substantially affect the location of our critical borders as seen in the bottom row of figure 3. Of course, there were cases for which there was a significant deviation between the smallest and largest stability border values for different combinations of the slow varying angles. This difference in the dynamical evolution of a planetary systems depending on the orientation of the orbits, however, is something well known in Celestial Mechanics (e.g. Michtchenko & Malhotra 2004; Hadjidemetriou 2006).

Figure 5 contains a collection of plots covering a large portion of our parameter space and providing a sense of how the various parameter combinations affect the location of the critical semi-major axes.

3.1. Fitting formulae

In order to quantify the results of our numerical experiments and provide a tool for assessing the stability status of a given system, we derived empirical formulae for the two critical borders over our entire parameter space. We tested models of first, second and third order in all parameters. By using a χ^2 goodness-of-fit test we evaluated how well our statistically derived empirical conditions reflected the simulation output. Some preliminary tests showed that, generally, a third order model in the independent variables fitted our data points better than the other models.

A third order fit with seven independent variables, however, has a large number of coefficients which we consider impractical. In order to reduce the size of the fit without compromising its accuracy and validity, we took the following course of action. In the first place, for every specific combination of M_b , M_p , I_m , e_b and e_p we recorded the highest

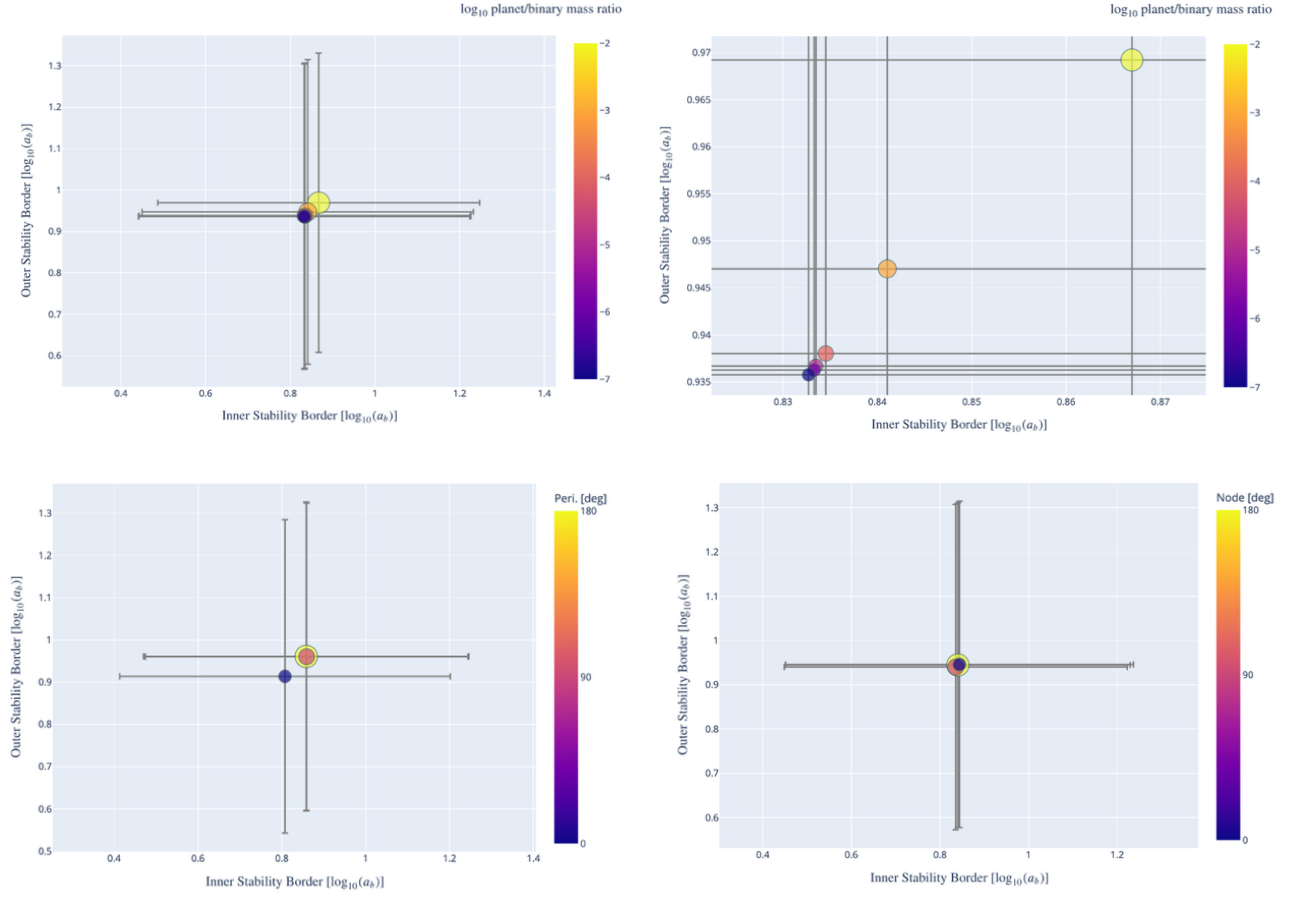


Figure 3. Same as Figure 2, but for the planet to binary mass ratio $M_p = m_p/(m_1 + m_2)$ (top left), a zoomed-in plot of the same (top right) the pericenter (bottom left), and the longitude of the ascending node (bottom right). In the parameter regime we have chosen for this study, the planet’s mass does not substantially affect the stability limits. Aligned pericenters lead to higher instability in a system. The relative position of the nodes does not significantly impact the location of stability limits.

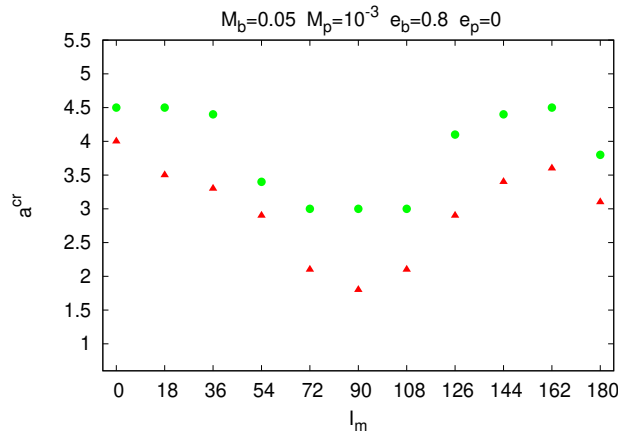


Figure 4. Critical semi-major axis against mutual inclination for system with $M_b = 0.05$, $M_p = 10^{-3}$, $e_b = 0.8$ and $e_p = 0$. The red color triangles represent the inner critical border while the green color circles indicates the outer one.

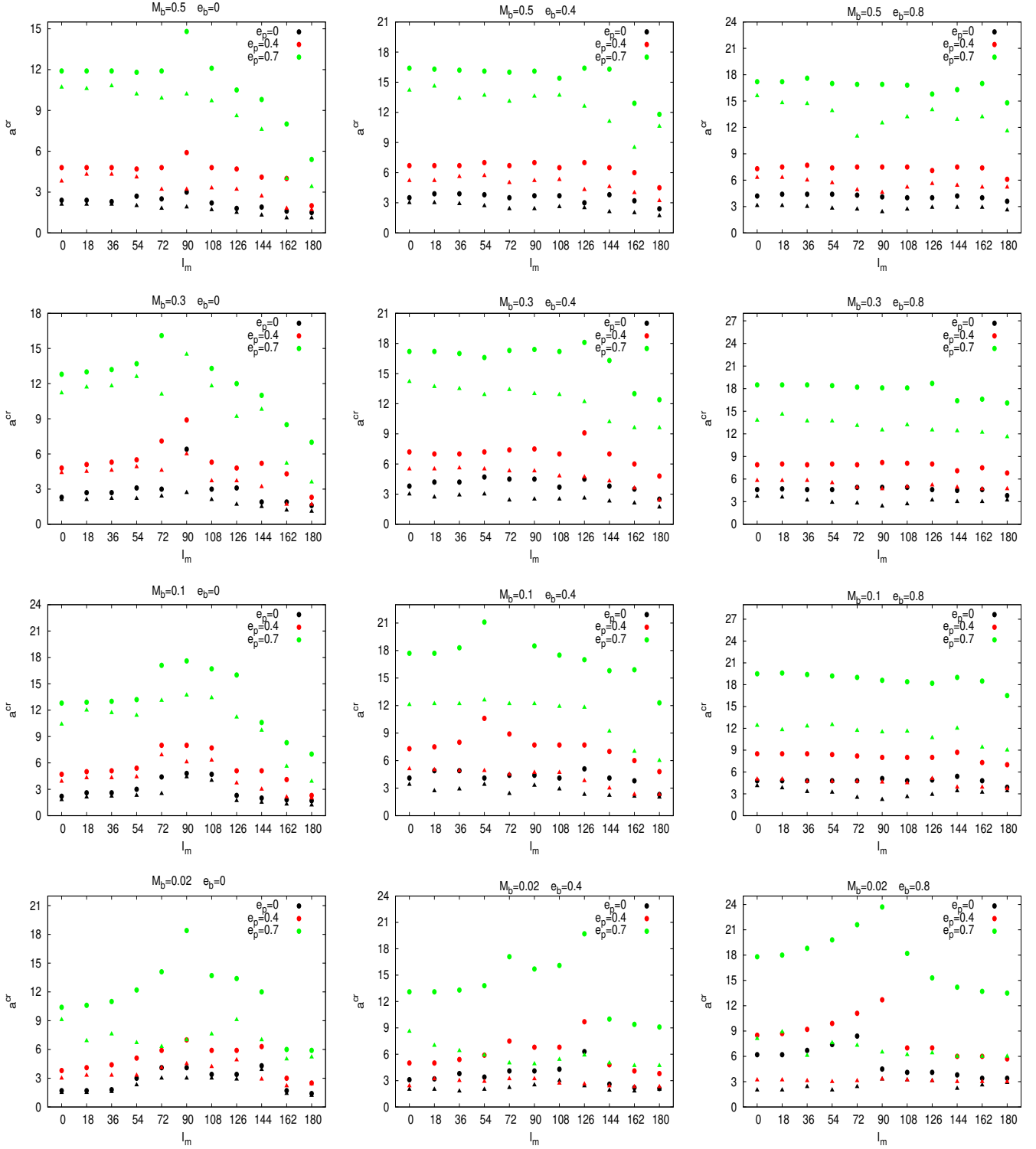


Figure 5. Critical semi-major axis against mutual inclination for various eccentricity values. The circles denote the outer limit (largest value recorded among the different combinations of the planetary pericenter and node), while the inner limit is represented by triangles (smallest value recorded). The colors correspond to different planetary eccentricity values. Finally, $M_p = 10^{-3}$.

outer border value among all pairs of $\Omega_p - \omega_p$, while for inner border we kept the smaller value. Apparently, for special configurations such as coplanar systems or three dimensional systems with initially circular planetary orbits we had only one slow varying angle to consider. Recording the extreme values of the critical axis among the results for the slow varying angle combinations and using them as input data to derive suitable fits, we eliminate two variables from the fitting process which results into a much smaller expression. In addition, the fitting formulae that will be obtained that way, will be closer to the physical meaning of our two dynamical borders we gave in section 2. Finally, we dropped the planetary mass from the fitting variables. As we saw earlier that the specific parameter had little effect on the critical distance. As can be seen from Figures 2 and 3 the difference between the impact of certain parameters on the stability borders can vary by several orders of magnitude. We, therefore, chose an exponential (base 10) form of the fit function. Finally, all angles were given in radians.

The fitting process was accomplished in two stages. In the first stage we derived a full third order model with respect to the remaining four parameters. In the second stage, we tried to reduce the size of the model while at the same time minimizing loss of accuracy. This was done by monitoring the reduced χ^2 parameter, i.e. $\chi_r^2 = \chi^2/(n-1)$, n being the number of data points. After we decided which terms we will keep in the new version of the model, we fitted the new reduced model to our data points. We would like to add here that, in order to provide better quality fits, we applied the above process on two data sets: the first one included planetary eccentricities of 0.8 or less while the second set included all values of the planetary eccentricity. This split was done in order to provide a better fit for the cases where $e_p \leq 0.8$ as the stability borders move up considerably when $e_p = 0.9$.

3.2. Empirical fits for $e_p \leq 0.8$

If planetary eccentricity is confined to $e_p \leq 0.8$, the inner and outer critical semi-major axes for the planet can be calculated using the following empirical fits:

$$a_i^{cr} = \bar{m} \cdot a_b \cdot 10^{[(\mathbf{B}_i \pm \mathbf{C}_i) \cdot \mathbf{X}_i]} \quad \text{and} \quad a_o^{cr} = \bar{m} \cdot a_b \cdot 10^{[(\mathbf{B}_o \pm \mathbf{C}_o) \cdot \mathbf{X}_o]}, \quad (7)$$

where \bar{m} is a correction factor that arises from the system of units used in the simulations, namely

$$\bar{m} = \left[\frac{m_1 + m_2 + m_p}{m_1 + m_2} \frac{1}{1 + m_p} \right]^{1/3} \quad (8)$$

and $(\mathbf{B}_{i,o} \pm \mathbf{C}_{i,o}) \cdot \mathbf{X}_{i,o}$ is the dot product between the fit coefficient vectors \mathbf{B} (along with their uncertainty vectors \mathbf{C}) and the parameter vectors \mathbf{X} for the inner and outer border, respectively. Those are

$$\begin{aligned} \mathbf{B}_i &= (0.20729, -0.32875, 0.10339, 0.58433, 0.36623, -0.25569, -0.06425, -0.38387, \\ &\quad 1.01951, 0.2691, 0.38912, -0.19863, -0.25361, -0.30333, 0.09080, -0.05955), \\ \mathbf{C}_i &= (0.003763, 0.01015, 0.00224, 0.00922, 0.00978, 0.00982, 0.00069, 0.00947, \\ &\quad 0.01176, 0.00687, 0.00759, 0.00420, 0.00735, 0.00913, 0.00129, 0.00280), \\ \mathbf{X}_i &= (1, M_{lb}, I_m, e_b, e_p, M_{lb}^2, I_m^2, e_b^2, e_p^2, M_{lb}e_b, M_{lb}e_p, I_me_b, M_{lb}e_b^2, M_{lb}e_p^2, I_m^2e_b, M_{lb}^3), \end{aligned} \quad (9)$$

where $M_{lb} = \log_{10}(M_b)$. For the outer critical planetary semi-major axis we find

$$\begin{aligned} \mathbf{B}_o &= (0.23612, -0.29377, 0.2271, 1.06753, 0.62109, -0.21512, -0.06648, -1.52936, \\ &\quad -0.4748, -0.31329, -0.00869, +0.11846, -0.03932, -0.00933, +0.87506, 1.25895), \\ \mathbf{C}_o &= (0.00317, 0.00927, 0.00313, 0.00905, 0.00975, 0.00910, 0.00202, 0.02330, \\ &\quad 0.02893, 0.00389, 0.00116, 0.00119, 0.00260, 0.00041, 0.01699, 0.02373), \\ \mathbf{X}_o &= (1, M_{lb}, I_m, e_b, e_p, M_{lb}^2, I_m^2, e_b^2, e_p^2, I_me_b, I_me_p, I_m^2e_b, M_{lb}^3, I_m^3, e_b^3, e_p^3). \end{aligned} \quad (10)$$

3.3. Empirical fits for the entire dataset

Making use of the same structure of equations (7) for the inner and outer critical semi-major axes, we find the following coefficients and parameters that cover the entire dataset for the inner critical semi-major axis of the planet:

$$\begin{aligned} \mathbf{B}_i &= (0.30889, -0.26446, 0.09362, 0.37426, 0.31306, -0.27007, -0.06102, -0.09262, \\ &\quad 0.19436, -0.18911, -0.05466, 0.06746, 0.08715, 1.19488), \\ \mathbf{C}_i &= (0.00398, 0.01150, 0.00238, 0.00688, 0.00286, 0.01061, 0.00073, 0.00472, \\ &\quad 0.00969, 0.00447, 0.00298, 0.00417, 0.00137, 0.00344), \\ \mathbf{X}_i &= (1, M_{lb}, I_m, e_b, e_p, M_{lb}^2, I_m^2, e_b^2, e_p^2, M_{lb}e_b, I_me_b, M_{lb}^3, M_{lb}^2e_b, I_m^2e_b, e_p^3). \end{aligned} \quad (11)$$

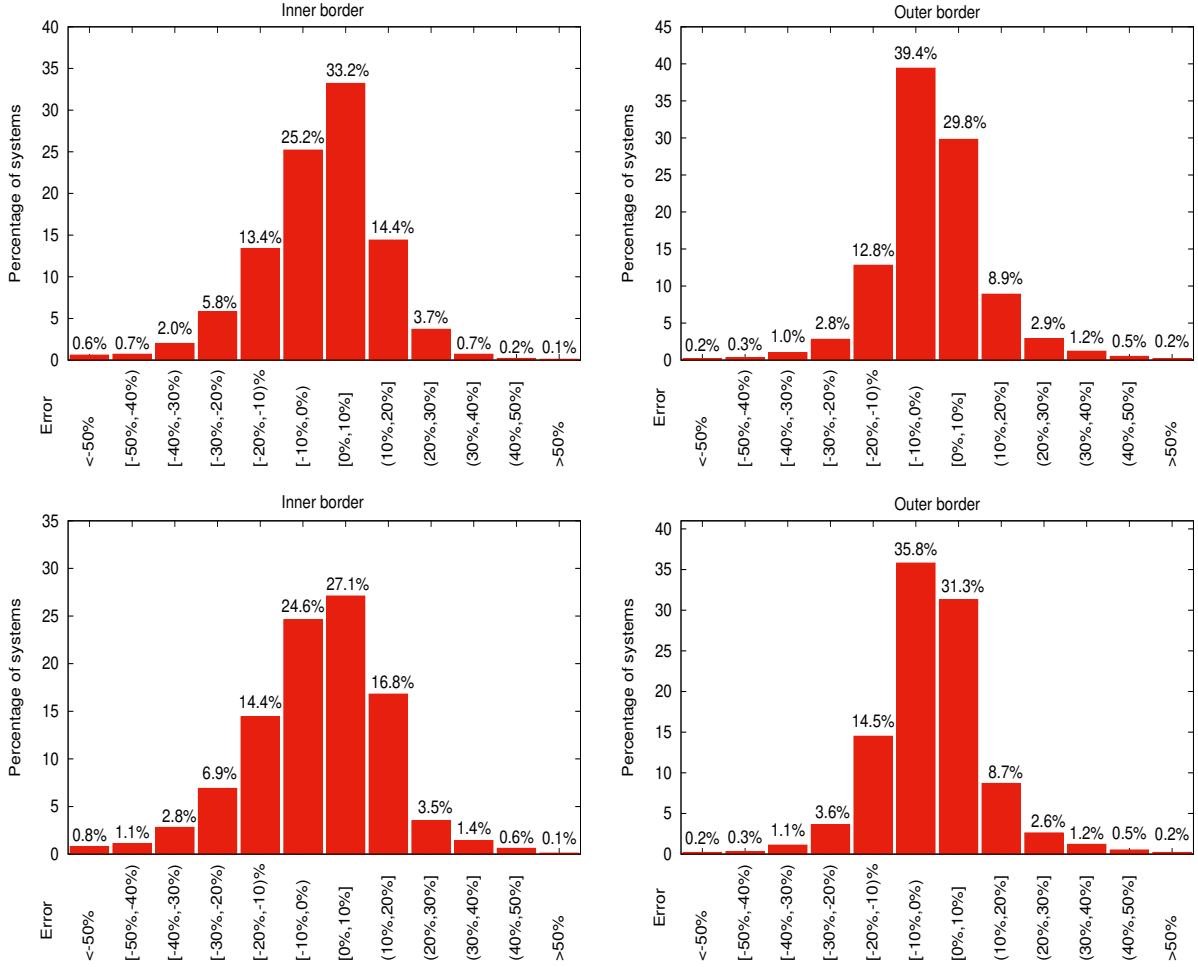


Figure 6. Error distribution from comparing our empirical fits against numerical simulation results. On the x-axis we have bins of relative percentage error between the results from the numerical simulations and the fits of equations (7), while in the y-axis we have the percentage of systems that fall into a specific error bin. The top row is for the $e_P \leq 0.8$ case, while the bottom row plots represent the more eccentric case.

For the outer critical semi-major axis of the planet we have:

$$\begin{aligned}
 \mathbf{B}_o &= (0.25556, -0.27038, 0.20643, 1.02175, 0.80028, -0.2101, -0.08452, -1.46178, -1.20652, \\
 &\quad -0.04965, -0.2989, -0.00227, -0.0386, 0.01838, 0.11341, 0.83529, 1.94189) \\
 \mathbf{C}_o &= (0.00324, 0.00888, 0.00285, 0.00861, 0.00844, 0.00865, 0.00086, 0.02216, \\
 &\quad 0.02216, 0.00176, 0.00370, 0.0010, 0.00247, 0.00054, 0.00113, 0.01616, 0.01616), \\
 \mathbf{X}_o &= (1, M_{lb}, I_m, e_b, e_p, M_{lb}^2, I_m^2, e_b^2, e_p^2, M_{lb}I_m, I_me_b, I_me_p, M_{lb}^3, M_{lb}I_m^2, I_m^2e_b, e_b^3, e_p^3).
 \end{aligned} \tag{12}$$

A visual representation of the quality of the empirical fits can be found in Figures 6 and 7. In Figure 6 we have a series of plots that show the distribution of the relative percentage error between the fits and the data points that the fits were based upon. In all cases, the majority of the errors are within $\pm 10\%$. Errors larger than 50% were encountered in less than two percent of all cases. Figure 7 demonstrates the effectiveness of our empirical formulae for a sample of combinations of masses and orbital eccentricities.

4. FIT PERFORMANCE AGAINST RANDOM SIMULATIONS

In order to test the quality of our fitting formulae, we carried out a set of 50000 additional simulations. The initial conditions for the additional simulations were created by using the pseudo-random number generating GNU Fortran

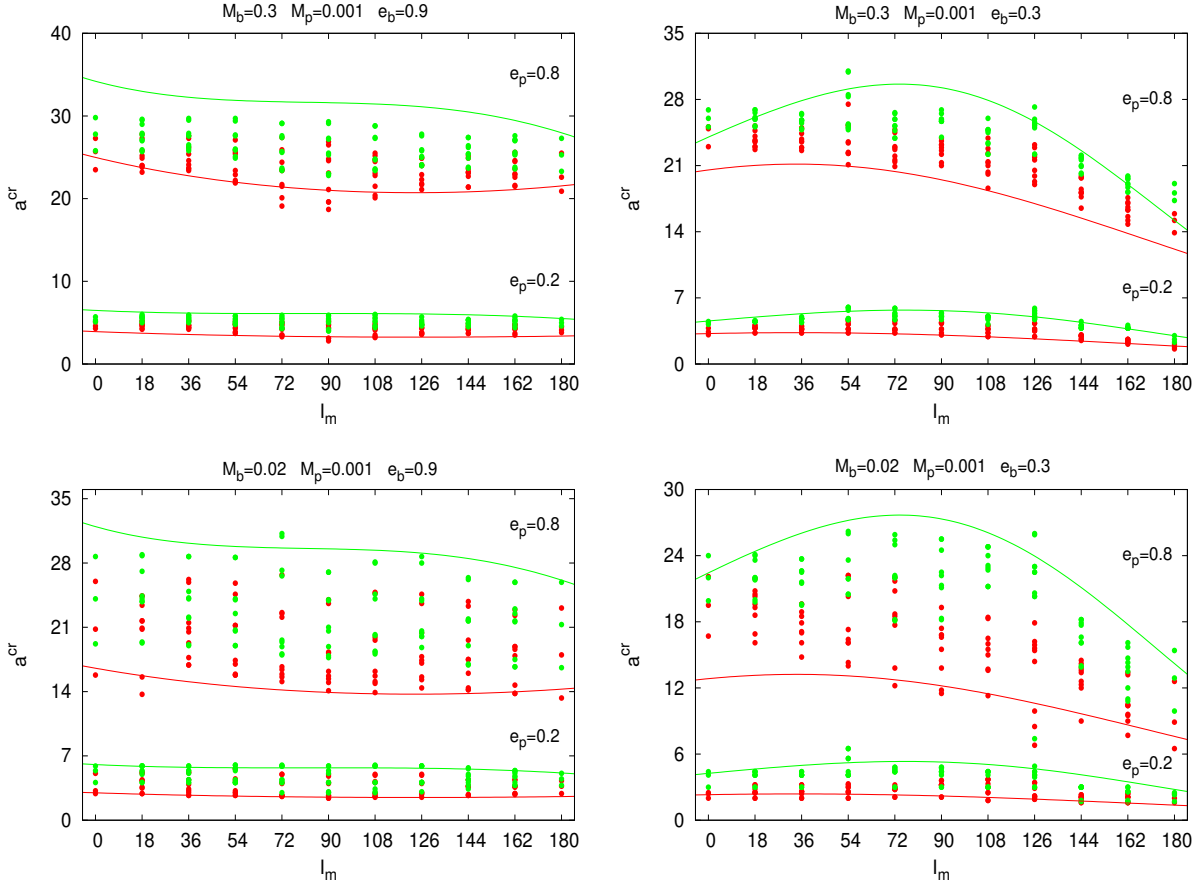


Figure 7. Critical semi-major axis ratio against mutual inclination for a variety of systems. The red color refers to the inner boundary, while the green colour denotes the outer stability border. The continuous lines are our empirical fits as given in subsection 3.2. The points are the output from the numerical simulations for the specific systems. Note that the majority of the points lie between the two curves as they ideally should.

function *rand*. The parameters were chosen within the ranges given in section 2, i.e. $M_b \in [0.01, 0.5]$, $M_p \in [10^{-7}, 10^{-2}]$, e_b and $e_p \in [0, 0.9]$, $I_m \in [0^\circ, 180^\circ]$, ϖ_p , ω_p and $\Omega_p \in [0^\circ, 360^\circ]$. In order to better target regions of interest, we sampled values for the planetary semimajor axis from two distributions that were constructed based on the location of the inner and outer critical borders as determined through our numerical integration grid. Rejection sampling allowed us to create a set of 25000 random systems based on the inner critical value distribution and another set of equal number of systems using the outer critical value distribution. The random seed number for the first set was 121, while for the other one the seed was 446.

The results of the random simulations and how they were classified based on our fitting formulae are presented in Tables (1) and (2). As stated in section 2, the planet is initiated at eight different positions around the binary, while the binary was started either at pericenter or at apocenter. That makes a total of sixteen initial positions for our systems. By definition, we would like to avoid encountering unstable orbits beyond the outer critical semi-major axis and any stable orbits below the inner critical semi-major axis. Therefore, we define our criteria for success as follows: the fits are predicting the stability of a system successfully when systems with 0 unstable positions were found in the stable zone, systems with 16 unstable positions were found in the unstable zone and finally, when all other cases were in between those two areas.

Generally, the outcome of the comparison between the fits and the results of the random system simulations was very good. If we consider the fits for $e_p \leq 0.8$, the majority of the fully stable and fully unstable systems was found in the right place. Only 1 case of a 0 and 54 cases of 16s were found in the wrong area (i.e. 0s in the fully unstable and 16s in the fully stable area). Also, 88.0% of the systems with mixed stability behavior were correctly classified.

Table 1. Random simulation result classification using the fits given in section 3.2.

INNER BORDER DISTRIBUTION				
N.U.I.P.	Stable	Quantity per zone		Total
		Mixed	Unstable	
0	12148(54.7%)	1826(8.2%)	1(0.0%)	13975(62.9%)
1 – 15	216(1.0%)	1825(8.2%)	32(0.1%)	2073(9.3%)
16	54(0.2%)	2245(10.1%)	3877(17.5%)	6176(27.8%)
Total	12418(55.9%)	5896(26.5%)	3910(17.6%)	22224(100.0%)

OUTER BORDER DISTRIBUTION				
N.U.I.P.	Stable	Quantity per zone		Total
		Mixed	Unstable	
0	14905(66.8%)	1712(7.7%)	2(0.0%)	16619(74.5%)
1 – 15	177(0.8%)	1468(6.5%)	18(0.1%)	1663(7.4%)
16	37(0.2%)	1685(7.5%)	2320(10.4%)	4042(18.1%)
Total	15119(67.8%)	4865(21.8%)	2340(10.5%)	22324(100.0%)

NOTE—N.U.I.P: Number of unstable initial positions of the planet on its initial orbit. The percentages refer to the number of individual cases over the total number of cases. For the interpretation of numbers in bold or color please see the main body of the paper.

In total, the success rate was 80.4%. The above mentioned numbers refer to the random systems that were drawn from the inner border distribution, but the pattern was very similar for the systems drawn from the outer border distribution. The success rate for those systems was 83.7%. The classification of the random systems for the restricted dataset can be found in Table 1, where the numbers in bold, when added up, provide the total success rate numbers mentioned above.

These percentages, however, are conservative estimates. This is because, as we saw with the results of the original set of simulations, a fully stable or a fully unstable system, at a specific semi-major axis, may occasionally appear in the mixed zone. In that case, we can add to the previous percentages the 0s and the 16s that are found in the mixed zone (the blue numbers in Table 1). When we do that, the 80.4% and 83.7% rise to 98.7% and 98.9% respectively. These numbers now represent the best case scenario. Nonetheless, we expect that the success rate would be somewhere between those extreme values as we do not know the exact location of the 0s and 16s since for a specific set of masses, inclination, eccentricities and slow angles we only have results for a specific semi-major axis and not a whole range as with our initial simulations that were used to derive the fits. As seen in Table 2, where the random simulation data are classified using fits to the entire dataset, the success prediction rates are very similar to those obtained in the case of the fits for $e_p \leq 0.8$.

5. EMPIRICAL FITTING WITH MACHINE LEARNING

While the fitting formulae provided above are accurate, they are nonetheless complex with many parameters. Hence, we opted to also train a Machine Learning model on our data set, allowing us to i) benchmark our analytical fits against another technique, and ii) provide a simple to use trained model as an alternative where the user does not have to manually implement the empirical formulae. We thus trained and tested an **XGBRegressor** model (Chen & Guestrin 2016) using its default hyperparameters on the same data set that the fits were based on. Similarly to what was done with the fits, we trained two separate models: one for planetary eccentricities $e_p \leq 0.8$ and one for $e_p \leq 0.9$. The goodness-of-fit of the models was initially evaluated through the mean absolute error of 10-fold cross-validations with the models trying to predict the inner and outer borders. We got values ranging from ~ 0.05 for the circular cases, to ~ 0.3 for

Table 2. Random simulation result classification using the fits given by equations in section 3.3.

INNER BORDER DISTRIBUTION				
N.U.I.P.	Stable	Quantity per zone		Total
		Mixed	Unstable	
0	13268(53.1%)	2009(8.0%)	2(0.0%)	15279(61.1%)
1 – 15	231(0.9%)	1955(7.8%)	90(0.4%)	2276(9.1%)
16	66(0.3%)	2513(10.1%)	4866(19.4%)	7445(29.8%)
Total	13565(54.3%)	6477(25.9%)	4958(19.8%)	25000(100.0%)

OUTER BORDER DISTRIBUTION				
N.U.I.P.	Stable	Quantity per zone		Total
		Mixed	Unstable	
0	16294(65.2%)	1791(7.1%)	2(0.0%)	18087(72.3%)
1 – 15	183(0.7%)	1552(6.2%)	57(0.3%)	1792(7.2%)
16	38(0.1%)	2014 (8.1%)	3069(12.3%)	5121(20.5%)
Total	16515(66.0%)	5357(21.4%)	3128(12.6%)	25000(100.0%)

NOTE—The notation, numbers and colors have the same meaning as in Table 1.

the eccentric cases, although those skewed by the MAE sensitivity to outliers. There were no significant differences for any given case between the MAE of the inner and outer borders. Moreover, a grid search over hyperparameters and testing other ML models such as **LightGBM** and **Random Forest Regressor** did not meaningfully improve the results. Figure 8 provides information of how well the Machine Learning models did against the data sets that were used to train them. The plots in that figure show that the errors of the Machine Learning models are more clustered towards the center of the bar charts compared to the same plots of the empirical fits in Figure 6.

As with our empirical formulae, we tested the Machine Learning models against the results from the random simulations we carried out. The results of that comparison are found in Tables 3 and 4. Generally, the results are in agreement and show similarities to those of the comparison between the empirical formulae and the random simulations. There are some differences though. First, there are more systems, from all categories, classified above the outer critical limit; about up to 2% more. Second, there are a bit more 16s in the zone between the two limits (of the order of 1%). These two differences imply that we have fewer 16s below the lower critical limit. Finally, in all but one case, we recorded more fully stable systems in the fully unstable area. But those cases were not many. Regarding the success rates, these seem to be similar to those scored by the empirical fits. The empirical formulae seem to do just a bit better (1%) in most of the cases. Hence, both approaches result in useful tools for characterizing the stability of circumbinary planets and may be used according to preference.

6. APPLICATION TO KNOWN CIRCUMBINARY PLANETARY SYSTEMS.

Among the exoplanets that have been discovered as of today, a number resides in circumbinary orbits. In this section we apply our stability criterion to the Kepler and Tess circumbinary systems that are currently known, i.e Kepler-16 (Doyle et al. 2011), Kepler-34 and Kepler-35 (Welsh et al. 2012), Kepler-38 (Orosz et al. 2012a), Kepler-47 (Orosz et al. 2012b, 2019), Kepler-64 (Schwamb et al. 2013; Kostov et al. 2013), Kepler-413 (Kostov et al. 2014), Kepler-453 (Welsh et al. 2015), Kepler-1647 (Kostov et al. 2016), Kepler-1661 (Socia et al. 2020), TIC 172900988 (Kostov et al. 2021) and TOI-1338 (Standing et al. 2023). In order to assess the stability status of the above systems we make use of the parameters given in the discovery papers. These parameter values can be found in Table 5.

Evaluating our empirical fits for the systems under investigation we find that all planets are near or beyond the outer critical semi-major axis. The values of the critical axes can be found in Table 6. Kepler-34 is the only exception with

Table 3. Random simulation result classification using the Machine Learning model ($e_p \leq 0.8$).

INNER BORDER DISTRIBUTION				
N.U.I.P.	Quantity per zone			
	Stable	Mixed	Unstable	Total
0	12658(57.0%)	1312(5.9%)	5(0.0%)	13975(62.9%)
1 – 15	382(1.7%)	1671(7.5%)	20(0.1%)	2073(9.3%)
16	133(0.6%)	2560(11.5%)	3483(15.7%)	6176(27.8%)
Total	13173(59.3%)	5543(24.9%)	3508(15.8%)	22224(100.0%)

OUTER BORDER DISTRIBUTION				
N.U.I.P.	Quantity per zone			
	Stable	Mixed	Unstable	Total
0	15415(69.1%)	1203(5.4%)	1(0.0%)	16619(74.5%)
1 – 15	300(1.3%)	1344(6.0%)	19(0.1%)	1663(7.4%)
16	99(0.5%)	1884(8.4%)	2059(9.2%)	4042(18.1%)
Total	15814(70.9%)	4431(19.8%)	2079(9.3%)	22324(100.0%)

NOTE—The notation, numbers and colours have the same meaning as in Tables 1 and 2.

Table 4. Random simulation result classification using the Machine Learning model ($e_p \leq 0.9$).

INNER BORDER DISTRIBUTION				
N.U.I.P.	Quantity per zone			
	Stable	Mixed	Unstable	Total
0	13630(54.5%)	1616(6.5%)	33(0.1%)	15279(61.1%)
1 – 15	435(1.8%)	1786(7.1%)	55(0.2%)	2276(9.1%)
16	182(0.7%)	2833(11.4%)	4430(17.7%)	7445(29.8%)
Total	14247(57.0%)	6235(25.0%)	4518(18.0%)	25000(100.0%)

OUTER BORDER DISTRIBUTION				
N.U.I.P.	Quantity per zone			
	Stable	Mixed	Unstable	Total
0	16592(66.3%)	1488(6.0%)	7(0.0%)	18087(72.3%)
1 – 15	328(1.3%)	1428(5.7%)	36(0.2%)	1792(7.2%)
16	166(0.7%)	2131(8.5%)	2824(11.3%)	5121(20.5%)
Total	17086(68.3%)	5047(20.2%)	2867(11.5%)	25000(100.0%)

NOTE—The notation, numbers and colors have the same meaning as in our previous Tables.

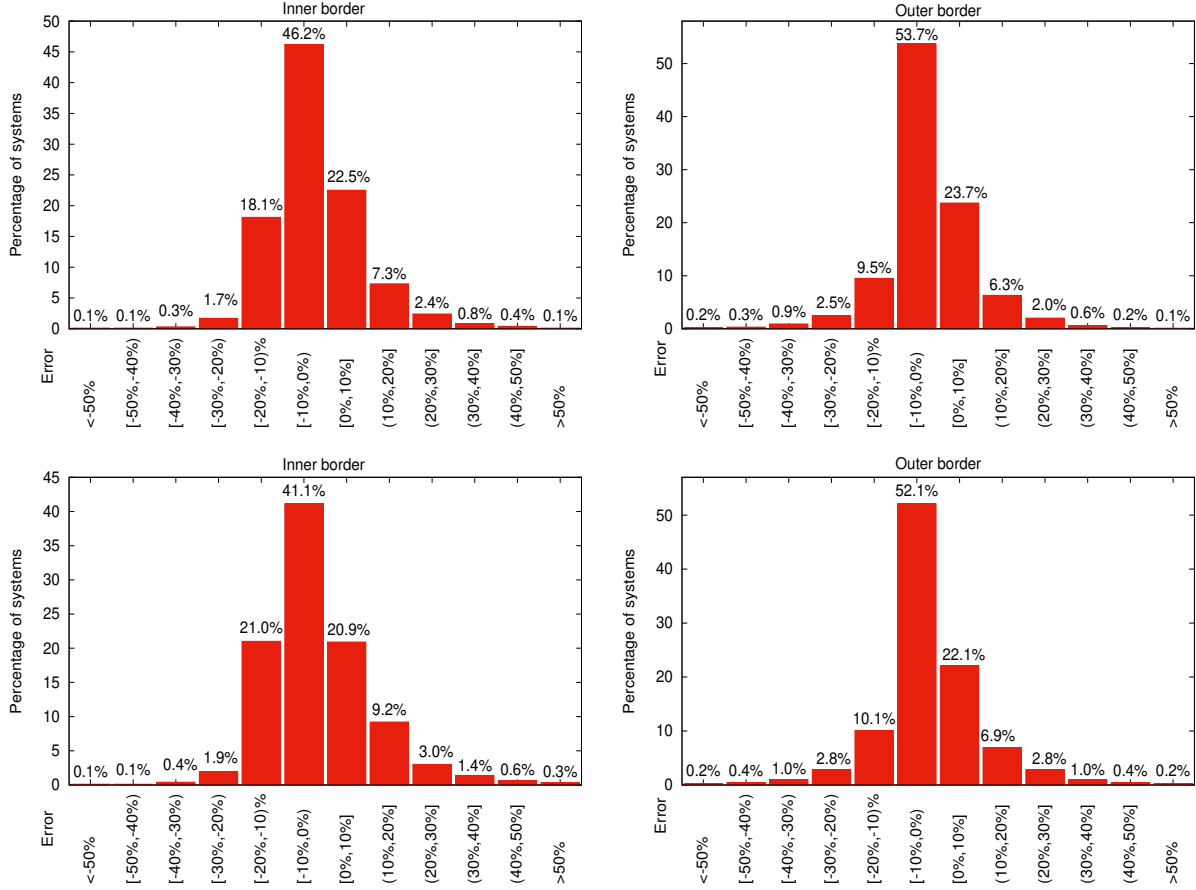


Figure 8. Error distribution from comparing the Machine Learning model against the results from the numerical simulations. On the x-axis we have bins of relative percentage error between the Machine Learning model and the results from the numerical simulations, while in the y-axis we have the percentage of systems that fall into a specific error bin. The top row corresponds to systems with $e_p \leq 0.8$ case, while the bottom row plots represent the more eccentric case.

its outer critical semi-major axis being 1.092 au, while the planet is located at 1.0896 au. Generally, these results are in agreement with stability analyses done in the discovery papers mentioned above and other papers that specifically focused on some of those circumbinary systems (e.g. Chavez et al. 2015; Popova & Shevchenko 2016).

We would like to point out, that, for this cursory analysis we neglected planet - planet interactions for the two multi-planet systems Kepler-47 and TOI-1338, i.e. we treated them as circumbinary systems having one planet at a time, i.e. we calculated the critical semi-major axes for one planet ignoring the presence of any other planet in the system. Regarding Kepler-47, Orosz et al. (2012b, 2019) (and references therein) state that the unstable area around the binary extends around 0.18 au which is in good agreement with what we have found. For TOI-1338c, as the inclination and the longitude of the node of the outer planet are not known, Standing et al. (2023) found that the system gets unstable for mutual inclinations $40^\circ < I_m < 120^\circ$. On the other hand, if we vary the mutual inclination in our fits, we notice that the outer planet always lies within the stable zone.

7. ONLINE PORTAL AND API

This section introduces a reboot of ExoStab (Pilat-Lohinger & Eggl 2011), the Exostab 2.0 Application Programming Interface (hereafter referred to as the API)². Exostab 2.0 is a software interface designed to facilitate interaction with large catalogs of numerical stability simulations such as constructed in this work. The API enables external programs and applications to access and utilize the functionalities of the stability catalog in a controlled and standardized manner.

² <https://exostab2.readthedocs.io/latest/>

Table 5. Circumbinary system parameter values.

System	$m_1(M_\odot)$	$m_2(M_\odot)$	$m_p(M_J)$	$I_m(^{\circ})$	$a_b(\text{au})$	$a_p(\text{au})$	e_b	e_p
Kepler-16	0.6897	0.20255	0.333	0.4	0.22431	0.7048	0.15944	0.00685
Kepler-34	1.0479	1.0208	0.22	1.81	0.22882	1.0896	0.52087	0.182
Kepler-35	0.8876	0.8094	0.127	1.28	0.17617	0.60345	0.1421	0.042
Kepler-38	0.949	0.249	0.384	0.182	0.1469	0.4646	0.1032	0.032
Kepler-47 (b)	0.957	0.342	0.006513	0.166	0.08145	0.2877	0.0288	0.021
Kepler-47 (c)	0.957	0.342	0.05984	1.165	0.08145	0.6992	0.0288	0.024
Kepler-47 (d)	0.957	0.342	0.00997	1.38	0.08145	0.9638	0.0288	0.044
Kepler-64	1.528	0.378	0.531	2.814	0.1744	0.634	0.2117	0.0539
Kepler-413	0.82	0.5423	0.21	4.073	0.10148	0.3553	0.0365	0.1181
Kepler-453	0.944	0.1951	0.05	2.258	0.18539	0.7903	0.0524	0.0359
Kepler-1647	1.21	0.975	1.52	2.9855	0.1276	2.7205	0.1593	0.0581
Kepler-1661	0.841	0.262	0.053	0.93	0.187	0.633	0.112	0.057
TIC 172900988	1.2388	1.2023	2.74	1.45	0.191928	0.89809	0.44793	0.088
TOI-1338 (b)	1.127	0.3313	0.0685	0	0.1321	0.4607	0.155522	0.088
TOI-1338 (c)	1.127	0.3313	0.205	0-180	0.1321	0.794	0.155522	0.16

Table 6. Stability borders for known circumbinary systems.

System	$a_i^{cr}(\text{au})$	$a_o^{cr}(\text{au})$	$a_p(\text{au})$
Kepler-16	0.551	0.688	0.7048
Kepler-34	0.804	1.092	1.0896
Kepler-35	0.410	0.511	0.60345
Kepler-38	0.349	0.427	0.4646
Kepler-47 (b)	0.178	0.198	0.2877
Kepler-47 (c)	0.179	0.200	0.6992
Kepler-47 (d)	0.181	0.206	0.9638
Kepler-64	0.457	0.627	0.634
Kepler-413	0.236	0.281	0.3553
Kepler-453	0.427	0.504	0.7903
Kepler-1647	0.310	0.397	2.7205
Kepler-1661	0.452	0.570	0.633
TIC 172900988	0.579	0.784	0.89809
TOI-1338 (b)	0.337	0.448	0.4607
TOI-1338 (c)	0.361	0.492	0.794

The API follows a RESTful architectural style, providing a well-defined set of endpoints for data retrieval, manipulation, and control. In particular, stability limits for system configurations can be queried for and the closest matches in our database are returned in JSON format. The reasonably dense catalog grid makes this process meaningful. The real advantage of returning nearest neighbors is the circumnavigation of issues that arise in fitting and interpolation, such as the mixing of dynamical behavior of systems in and out of resonance, etc. Only stability limits that were actually

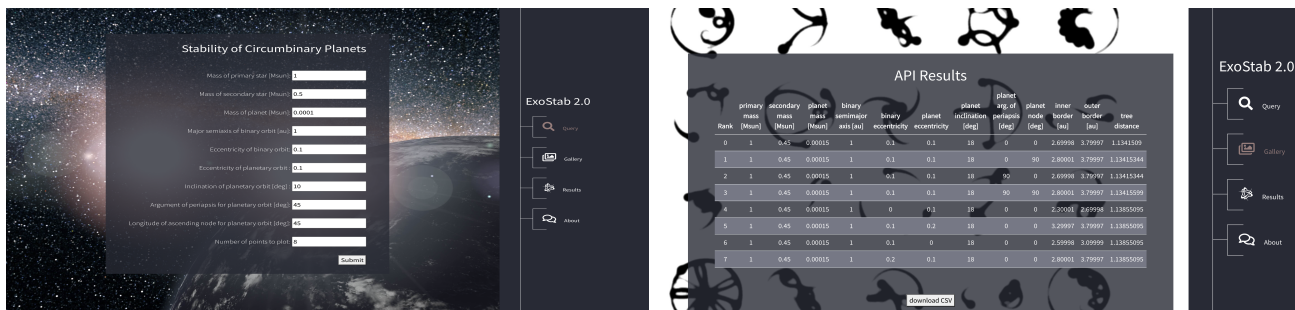


Figure 9. Web-based front-end for Exostab 2.0 API.

calculated are being returned. A web-based front-end³ allows for convenient visualization and access to query results in a formatted table as well as through as CSV file download (see figure 9).

8. DISCUSSION

The study of planetary motion in stellar binaries and the search for a way to identify stable and unstable systems dates back several decades. The following subsection provides some relevant context to this study.

8.1. Historical context and state-of-the-art

Harrington (1977) investigated the problem by carrying out a limited number of numerical simulations of three body systems consisting of a stellar binary and a planet. Based on his numerical results, he derived an empirical condition for identifying stable planetary orbits in stellar binaries. A few years later, Dvorak (1986) investigated the problem of stable and unstable circumbinary motion in the the context of the planar elliptic restricted three body problem with equal mass primaries. He integrated numerically a number of circumbinary orbits for 500 binary periods and a planetary orbit was considered stable if its eccentricity remained smaller than 0.3 throughout the whole integration time. He derived two empirical formulae representing the Lower Critical Orbit (LCO) and the Upper Critical Orbit (UCO). These borders correspond to our inner and outer critical semi-major axis respectively.

The most widely used empirical criterion has been the one presented in Holman & Wiegert (1999). They investigated the stability of planets in binary systems, either in circumstellar or circumbinary orbits. For the circumbinary case, they ran numerical simulations of massless particles on initially circular and prograde orbits in the binary plane of motion and with different initial orbital longitudes. The binary mass ratio was taken in the range 0.1-0.9 and the binary eccentricity in the range 0-0.7. The simulation time was set to 10000 binary periods. If a particle survived the whole integration time at all initial longitudes, then the system was classified as stable. The semi-major axis closest to the binary at which the massless particle was stable at all initial orbital longitudes was called the critical semi-major axis and was given by (using our notation):

$$a_h = [1.60 + 5.10e_b - 2.22e_b^2 + 4.12M_b - 4.27e_bM_b - 5.09M_b^2 + 4.61e_b^2M_b^2]a_b. \quad (13)$$

In many cases, however, 'islands' of instability were noticed at values greater than the critical semi-major axis. This was mainly due to the choice the authors of that study made in terms of how they defined the critical semi-major axis. According to the way we defined our critical distances, such a system would be classified into the mixed stability behavior zone.

The work of Holman & Wiegert (1999) was subsequently extended by Quarles et al. (2018). In that work, a number of circumbinary systems was numerically simulated with many parameter ranges widened, i.e the binary mass ratio acquired values between 0.01 and 0.5 with a step of 0.01, the binary eccentricity was given values between 0 and 0.8 with a step of 0.01 and the integration time was set to 10^5 binary periods. Finally, the planetary mean anomaly was given values between 2° and 180° with a step of 2° . The definition of stability remained the same as in Holman & Wiegert (1999). Eventually, Quarles et al. (2018) provided two fits for the critical semi-major axis of similar form to the one in Holman & Wiegert (1999)

³ <https://apexgroup.web.illinois.edu/stability/index.html>

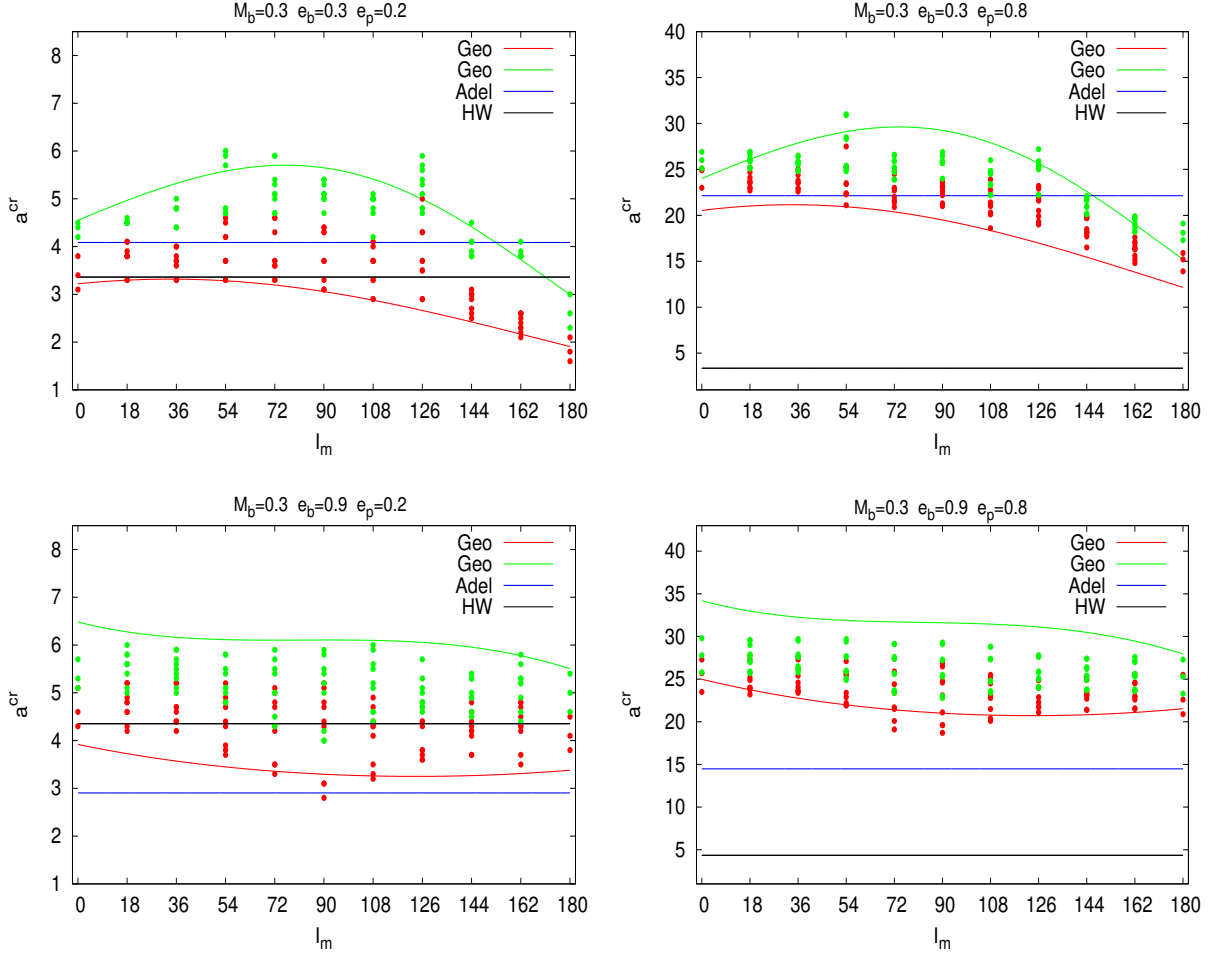


Figure 10. Comparison between different stability fits. Geo stands for the fits of the present work, Adel denotes the work by [Adelbert et al. \(2023\)](#) and HW denotes the classification formula given in [Holman & Wiegert \(1999\)](#). As previously, the green color denotes the outer critical border, while the red color represents the inner critical border. The circles are the results from our numerical simulations.

Finally, [Adelbert et al. \(2023\)](#), in the context of coorbital planets around stellar binaries, they performed numerical simulations of planets moving in the plane of the binary. They considered the same binary mass ratios as [Holman & Wiegert \(1999\)](#) but their highest binary eccentricity was only 0.5. A step forward compared to previous studies was the consideration of planetary eccentricity (up to 0.9). Unfortunately, although not very clear, it appears though that the planet was always initialized at the same single position and therefore the potential effect of different initial mean or true anomalies could not be evaluated. The integration time was 10^5 binary orbits and a system was considered unstable if the planetary semi-major axis exhibited a variation of more than 20% compared to its initial value. They reached the following best fit based on their data:

$$a_{ad} = [1.36 + 5.79e_b - 5.87e_b^2 + 1.99M_b - 3.14M_b^2 + (1.85 - 2.10e_b^2 + 3.0e_b\mu_b)e_p] \frac{a_b}{1 - e_p}. \quad (14)$$

As we can see, all the above circumbinary stability criteria cover only part of the parameter space. Also, the definition of stability they are based on, results, on several occasions, in characterizing circumbinary planets as stable while they are actually unstable and vice versa. Figure 10 is a graphical comparison among the criteria in [Holman & Wiegert \(1999\)](#) and [Adelbert et al. \(2023\)](#) and the fits presented in this work for some parameter combinations. It is clear that [Holman & Wiegert \(1999\)](#) fails completely as planetary eccentricity increases, while [Adelbert et al. \(2023\)](#) does better but it still has its own limitations, such as for example when the binary eccentricity gets high.

8.2. *Relativistic and tidal effects*

Other effects than Newtonian gravity, such as the relativistic precession of the binary pericenter or tidal friction between the two stars, can be of importance for the orbital evolution of the entire system (e.g. [Naoz et al. 2013](#); [Correia et al. 2016](#)). Tidal friction between the stars may eventually shrink the binary orbit and reduce its eccentricity. Depending on the distance between the stars, the timescale for any orbital changes that may eventually affect the planetary orbit can be quite long. For instance, the eccentricity and semi-major axis of Kepler-34 reduced by about 5% and 3% respectively after 8 Gyr ([Chavez et al. 2015](#)). On the other hand, depending on the system parameters, the relativistic precession of the pericenter can operate on timescales comparable to our integration time of 10^6 planetary periods and have an effect on the orbital evolution of the planet ([Migaszewski & Goździewski 2011](#); [Georgakarakos & Eggl 2015](#)). The pericentre of Kepler-34 was found to circulate with a period of around $2 \cdot 10^5$ years ([Chavez et al. 2015](#)), while the integration time that corresponds to Kepler-34b, if we were to simulate the system within the context of this work, is around $7.9 \cdot 10^5$ years. However, previous studies investigated the dynamical evolution of circumbinary planets away from mean motion resonances with the binary, considering mainly secular effects. As we mentioned in section 3, one key process to three body system instability is the overlapping of adjacent mean motion resonances ([Wisdom 1980](#); [Mudryk & Wu 2006](#); [Deck et al. 2013](#); [Ramos et al. 2015](#); [Hadden & Lithwick 2018](#)). Therefore, the dynamical evolution of circumbinary systems that are near mean motion resonances may deviate from that in systems dominated by secular effects and relativistic pericenter precession. The precise impact of relativity and tidal interaction on circumbinary systems is, therefore, a topic of ongoing research.

9. SUMMARY AND CONCLUSIONS

In this work, we have investigated the problem of dynamical stability of circumbinary orbits subject to Newtonian gravity. We have carried out more than $3 \cdot 10^8$ of highly accurate numerical simulations of three dimensional and eccentric systems considering a wide range of mass ratios that are relevant to the study of circumbinary planets. Eccentricities of both the binary and the planetary orbits in our study range from 0-0.9. Regarding the masses used in our simulations, for the inner binary we considered systems featuring equal mass stars down to mass ratios of 0.01 to account for situations where we may have a star close to the minimum required mass for the onset of nuclear fusion. For the outer perturber, i.e. the circumbinary planet, we explored mass ratios that would be valid from brown dwarf like bodies down to Mercury mass planets. Our numerical experiments were carried out over a timescale of one million planetary orbital periods, which is one of the longest integration times ever performed in similar studies. This allows us to capture dynamical effects that require some time to build up (e.g. secular resonances) and affect the planetary orbit. We classified the parameter space into three stability regimes separated by critical borders: a zone where investigated orbits were fully stable, a zone where investigated orbits were fully unstable and one with mixed behaviour. The location of the critical borders was mainly affected by the eccentricities of the binary and planetary orbits, the mass ratio of the binary and the mutual inclination between the binary and planetary orbital planes. Based on the results of the numerical simulations we derived empirical formulae for the critical semi-major axes of circumbinary planetary systems as a function of the system parameters that identify whether or not a configuration is dynamically stable over a million planetary orbits. We have developed two sets of fitting formulae: one for planetary eccentricities up to 0.8 and one for planetary eccentricities as high as 0.9. The former exhibits a better performance in terms of stability classification for most systems, while the latter is meant to cover the entire investigated parameter space.

We have also trained Machine Learning (ML) models on our data set and compared their performance in predicting dynamical stability in circumbinary systems. The empirical formulae and the Machine Learning models were tested against results from numerical simulations of randomly chosen circumbinary systems. Both ML and empirical classifiers show similar performance, and constitute a vast improvement over existing techniques, in particular over [Holman & Wiegert \(1999\)](#), in terms of parameter space covered. Finally, we tested our empirical stability criteria against known Kepler and TESS systems. The results showed excellent agreement with the real systems. We have also discussed the impact of relativity and tidal interactions.

As our simulations and subsequent results are based on Newtonian gravity and dimensionless mass ratios, they are applicable to any gravitational system compatible with such a model. Our predictive tools may, thus, be used in various astrophysical contexts, such as planet formation studies, minor planets with moonlets in the solar system as well as the detection and characterization of circumbinary planets in the hunt for habitable worlds.

REFERENCES

- Adelbert, S., Penzlin, A. B. T., Schäfer, C. M., et al. 2023, *A&A*, 680, A29, doi: [10.1051/0004-6361/202244329](https://doi.org/10.1051/0004-6361/202244329)
- Chavez, C. E., Georgakarakos, N., Prodan, S., et al. 2015, *MNRAS*, 446, 1283, doi: [10.1093/mnras/stu2142](https://doi.org/10.1093/mnras/stu2142)
- Chen, C., Lubow, S. H., & Martin, R. G. 2020, *MNRAS*, 494, 4645, doi: [10.1093/mnras/staa1037](https://doi.org/10.1093/mnras/staa1037)
- Chen, T., & Guestrin, C. 2016, arXiv e-prints, arXiv:1603.02754, doi: [10.48550/arXiv.1603.02754](https://doi.org/10.48550/arXiv.1603.02754)
- Childs, A. C., & Martin, R. G. 2021, *MNRAS*, 507, 3461, doi: [10.1093/mnras/stab2419](https://doi.org/10.1093/mnras/stab2419)
- Chirikov, B. V. 1979, *Physics Reports*, 52, 263, doi: [https://doi.org/10.1016/0370-1573\(79\)90023-1](https://doi.org/10.1016/0370-1573(79)90023-1)
- Correia, A. C. M., Boué, G., & Laskar, J. 2016, *Celestial Mechanics and Dynamical Astronomy*, 126, 189, doi: [10.1007/s10569-016-9709-9](https://doi.org/10.1007/s10569-016-9709-9)
- Deck, K. M., Payne, M., & Holman, M. J. 2013, *ApJ*, 774, 129, doi: [10.1088/0004-637X/774/2/129](https://doi.org/10.1088/0004-637X/774/2/129)
- Doolin, S., & Blundell, K. M. 2011, *MNRAS*, 418, 2656, doi: [10.1111/j.1365-2966.2011.19657.x](https://doi.org/10.1111/j.1365-2966.2011.19657.x)
- Doyle, L. R., Carter, J. A., Fabrycky, D. C., et al. 2011, *Science*, 333, 1602, doi: [10.1126/science.1210923](https://doi.org/10.1126/science.1210923)
- Dvorak, R. 1986, *A&A*, 167, 379
- Dvorak, R., Froeschle, C., & Froeschle, C. 1989, *A&A*, 226, 335
- Georgakarakos, N. 2008, *Celestial Mechanics and Dynamical Astronomy*, 100, 151, doi: [10.1007/s10569-007-9109-2](https://doi.org/10.1007/s10569-007-9109-2)
- . 2013, *NewA*, 23, 41, doi: [10.1016/j.newast.2013.02.004](https://doi.org/10.1016/j.newast.2013.02.004)
- . 2022, *MNRAS*, 511, 4396, doi: [10.1093/mnras/stab3332](https://doi.org/10.1093/mnras/stab3332)
- Georgakarakos, N., & Eggl, S. 2015, *ApJ*, 802, 94, doi: [10.1088/0004-637X/802/2/94](https://doi.org/10.1088/0004-637X/802/2/94)
- Georgakarakos, N., Eggl, S., & Dobbs-Dixon, I. 2021, *Frontiers in Astronomy and Space Sciences*, 8, 44, doi: [10.3389/fspas.2021.640830](https://doi.org/10.3389/fspas.2021.640830)
- Hadden, S., & Lithwick, Y. 2018, *AJ*, 156, 95, doi: [10.3847/1538-3881/aad32c](https://doi.org/10.3847/1538-3881/aad32c)
- Hadjidemetriou, J. D. 2006, *Celestial Mechanics and Dynamical Astronomy*, 95, 225
- Harrington, R. S. 1977, *AJ*, 82, 753, doi: [10.1086/112121](https://doi.org/10.1086/112121)
- Holman, M. J., & Wiegert, P. A. 1999, *AJ*, 117, 621, doi: [10.1086/300695](https://doi.org/10.1086/300695)
- Hong, C., & van Putten, M. H. P. M. 2021, *NewA*, 84, 101516, doi: [10.1016/j.newast.2020.101516](https://doi.org/10.1016/j.newast.2020.101516)
- Janson, M., Hormuth, F., Bergfors, C., et al. 2012, *ApJ*, 754, 44, doi: [10.1088/0004-637X/754/1/44](https://doi.org/10.1088/0004-637X/754/1/44)
- Kenyon, S. J., & Bromley, B. C. 2021, *AJ*, 161, 211, doi: [10.3847/1538-3881/abe858](https://doi.org/10.3847/1538-3881/abe858)
- Kostov, V. B., McCullough, P. R., Hinse, T. C., et al. 2013, *ApJ*, 770, 52, doi: [10.1088/0004-637X/770/1/52](https://doi.org/10.1088/0004-637X/770/1/52)
- Kostov, V. B., McCullough, P. R., Carter, J. A., et al. 2014, *ApJ*, 784, 14, doi: [10.1088/0004-637X/784/1/14](https://doi.org/10.1088/0004-637X/784/1/14)
- Kostov, V. B., Orosz, J. A., Welsh, W. F., et al. 2016, *ApJ*, 827, 86, doi: [10.3847/0004-637X/827/1/86](https://doi.org/10.3847/0004-637X/827/1/86)
- Kostov, V. B., Powell, B. P., Orosz, J. A., et al. 2021, *AJ*, 162, 234, doi: [10.3847/1538-3881/ac223a](https://doi.org/10.3847/1538-3881/ac223a)
- Lam, C., & Kipping, D. 2018, *MNRAS*, 476, 5692, doi: [10.1093/mnras/sty022](https://doi.org/10.1093/mnras/sty022)
- Mardling, R. A. 2008, in *The Cambridge N-Body Lectures*, ed. S. J. Aarseth, C. A. Tout, & R. A. Mardling, Vol. 760, 59, doi: [10.1007/978-1-4020-8431-7_3](https://doi.org/10.1007/978-1-4020-8431-7_3)
- Mardling, R. A. 2013, *Monthly Notices of the Royal Astronomical Society*, 435, 2187, doi: [10.1093/mnras/stt1438](https://doi.org/10.1093/mnras/stt1438)
- Michtchenko, T. A., & Malhotra, R. 2004, *Icarus*, 168, 237, doi: [10.1016/j.icarus.2003.12.010](https://doi.org/10.1016/j.icarus.2003.12.010)
- Migaszewski, C., & Goździewski, K. 2011, *MNRAS*, 411, 565, doi: [10.1111/j.1365-2966.2010.17702.x](https://doi.org/10.1111/j.1365-2966.2010.17702.x)
- Mikkola, S. 1997, *Celestial Mechanics and Dynamical Astronomy*, 67, 145, doi: [10.1023/A:1008217427749](https://doi.org/10.1023/A:1008217427749)
- Mudryk, L. R., & Wu, Y. 2006, *ApJ*, 639, 423, doi: [10.1086/499347](https://doi.org/10.1086/499347)
- Naoz, S., Kocsis, B., Loeb, A., & Yunes, N. 2013, *The Astrophysical Journal*, 773, 187, doi: [10.1088/0004-637X/773/2/187](https://doi.org/10.1088/0004-637X/773/2/187)
- Offner, S. S. R., Moe, M., Kratter, K. M., et al. 2022, arXiv e-prints, arXiv:2203.10066, <https://arxiv.org/abs/2203.10066>
- Orosz, J. A., Welsh, W. F., Carter, J. A., et al. 2012a, *ApJ*, 758, 87, doi: [10.1088/0004-637X/758/2/87](https://doi.org/10.1088/0004-637X/758/2/87)
- . 2012b, *Science*, 337, 1511, doi: [10.1126/science.1228380](https://doi.org/10.1126/science.1228380)
- Orosz, J. A., Welsh, W. F., Haghighipour, N., et al. 2019, *AJ*, 157, 174, doi: [10.3847/1538-3881/ab0ca0](https://doi.org/10.3847/1538-3881/ab0ca0)
- Pilat-Lohinger, E., & Eggl, S. 2011, *Publications of the Astronomy Department of the Eotvos Lorand University*, 20, 135
- Pilat-Lohinger, E., Funk, B., & Dvorak, R. 2003, *A&A*, 400, 1085, doi: [10.1051/0004-6361:20021811](https://doi.org/10.1051/0004-6361:20021811)
- Popova, E. A., & Shevchenko, I. I. 2016, *Astronomy Letters*, 42, 474, doi: [10.1134/S1063773716060050](https://doi.org/10.1134/S1063773716060050)
- Quarles, B., Satyal, S., Kostov, V., Kaib, N., & Haghighipour, N. 2018, *ApJ*, 856, 150, doi: [10.3847/1538-4357/aab264](https://doi.org/10.3847/1538-4357/aab264)
- Raghavan, D., McAlister, H. A., Henry, T. J., et al. 2010, *ApJS*, 190, 1, doi: [10.1088/0067-0049/190/1/1](https://doi.org/10.1088/0067-0049/190/1/1)
- Ramos, X. S., Correa-Otto, J. A., & Beaugé, C. 2015, *Celestial Mechanics and Dynamical Astronomy*, 123, 453, doi: [10.1007/s10569-015-9646-z](https://doi.org/10.1007/s10569-015-9646-z)

- Schwamb, M. E., Orosz, J. A., Carter, J. A., et al. 2013, *ApJ*, 768, 127, doi: [10.1088/0004-637X/768/2/127](https://doi.org/10.1088/0004-637X/768/2/127)
- Shevchenko, I. I. 2015, *ApJ*, 799, 8, doi: [10.1088/0004-637X/799/1/8](https://doi.org/10.1088/0004-637X/799/1/8)
- Socia, Q. J., Welsh, W. F., Orosz, J. A., et al. 2020, *AJ*, 159, 94, doi: [10.3847/1538-3881/ab665b](https://doi.org/10.3847/1538-3881/ab665b)
- Standing, M. R., Sairam, L., Martin, D. V., et al. 2023, *Nature Astronomy*, 7, 702, doi: [10.1038/s41550-023-01948-4](https://doi.org/10.1038/s41550-023-01948-4)
- Sundman, K. 1913, *Acta Math.*, 36, 105, doi: [10.1007/BF02422379](https://doi.org/10.1007/BF02422379)
- Welsh, W. F., Orosz, J. A., Carter, J. A., et al. 2012, *Nature*, 481, 475, doi: [10.1038/nature10768](https://doi.org/10.1038/nature10768)
- Welsh, W. F., Orosz, J. A., Short, D. R., et al. 2015, *ApJ*, 809, 26, doi: [10.1088/0004-637X/809/1/26](https://doi.org/10.1088/0004-637X/809/1/26)
- Wisdom, J. 1980, *AJ*, 85, 1122, doi: [10.1086/112778](https://doi.org/10.1086/112778)